Original Article

Effect of flapless osteoperforation-assisted tooth movement on atrophic alveolar ridge: Histomorphometric and gene-enrichment analysis

Ji-Won Lee[a]; Jung-Yul Cha[b]; Ki-Ho Park[c]; Yoon-Goo Kang[c]; Su-Jung Kim[c]

ABSTRACT

Objective: To investigate the effect of flapless osteoperforation on the tissue response of the atrophic alveolar ridge affected by orthodontic tooth movement (OTM).

Materials and Methods: An atrophic alveolar ridge model was established in the mandibular quadrants of eight beagle dogs. As a split-mouth design, the quadrants were randomly divided into group C (OTM only) and group OP (OTM with flapless osteoperforation). The rate of OTM for 10 weeks was compared between groups, and micro-CT-based histomorphometric analysis and RNA-sequencing-based gene-enrichment analysis were performed targeting the atrophic ridge.

Results: Group OP displayed more rapid tooth movement with lower bone mineral density and higher trabecular fraction in the atrophic ridge than did group C, showing no intergroup difference of total ridge volume. As contributing biological functional pathways in group OP, the genes related to osteoclast differentiation and TNF signaling pathway were up-regulated and those associated with Wnt signaling pathway and AMPK signaling pathway were down-regulated.

Conclusions: Flapless osteoperforation facilitated the rate of OTM toward the atrophic ridge, maintaining low bone density, whereas it did not increase the volume of the atrophic ridge. (*Angle Orthod.* 2018;88:82–90.)

KEY WORDS: Flapless-osteoperforation; Orthodontic tooth movement; Atrophic alveolar ridge; Histomorphometric analysis; Gene-enrichment analysis

INTRODUCTION

A common sequela of tooth extraction is residual ridge resorption due to intra-alveolar socket remodeling and extra-alveolar surface modeling.[1] The intra-alveolar socket is occupied by woven bone in the early stages and replaced by dense lamellar bone with bone marrow cavities. Meanwhile, thickness and height of the extra-alveolar bony wall decrease by surface resorption from the periosteum due to the absence of bundle bone and the periodontal ligament, creating functional loads. Consequently, ridge reduction tends to be greater in the transverse than in the vertical dimension and transverse resorption is more prominent on the buccal than on the lingual side,[2] which creates an unfavorable periodontal condition impeding orthodontic tooth movement (OTM).

With a view to move teeth through the atrophic ridge, various surgical procedures have been introduced.[3–5] Ridge augmentation procedures have been applied to improve periodontal dimensions around the moving tooth toward the atrophic ridge,[3,4] recently in conjunction with tissue-engineering techniques.[5] However, this procedure requires invasive surgical insult and a postsurgical waiting period for graft stabilization before initiating OTM while retaining risks of graft failure and root resorption.[3] As a minimally invasive approach, flapless decortication such as corticision,[6] piezocision,[7] piezopuncture,[8] and micro-osteoperforation[9] has been attempted to preserve periosteal blood supply and surrounding soft tissues to minimize external ridge resorption while activating internal remodeling of bone and the periodontal ligament to elicit a regional acceleratory phenomenon (RAP). Nonetheless, evaluations have focused on the rate of OTM when

[a] Postgraduate Student, Kyung Hee University Graduate School, Seoul, Korea.

[b] Associate Professor, Department of Orthodontics, Yonsei University School of Dentistry, Seoul, Korea.

[c] Associate Professor, Department of Orthodontics, Kyung Hee University School of Dentistry, Seoul, Korea.

Corresponding author: Dr Su-Jung Kim, Department of Orthodontics, Oral Biology Research Institute, Kyung Hee University School of Dentistry, 1 Hoegi-Dong, Dongdaemoon-Ku, Seoul 130-701, Korea
(e-mail: ksj113@khu.ac.kr)

Accepted: August 2017. Submitted: June 2017.
Published Online: October 10, 2017

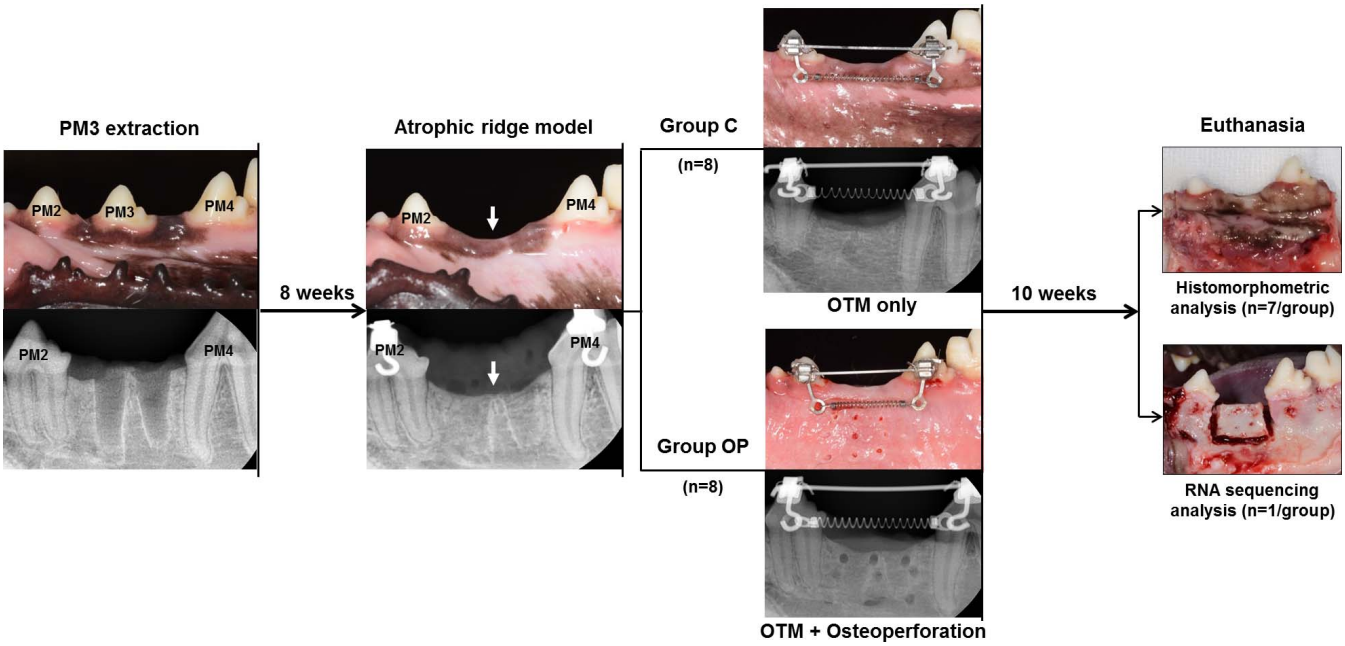

Figure 1. Diagram of the experimental design in the beagle model with the atrophic ridge (indicated by arrow); PM2, second premolar; PM4, fourth premolar.

supported by sound periodontium, with no special consideration for the tissue responses of the atrophic alveolar ridge.

Micro-osteoperforation has recently been proposed as a minimally invasive way to facilitate tooth movement by increasing the levels of cytokine expression and thereby local osteoporotic changes around the target teeth.[9,10] This technique has clinical benefits including no need for flap reflection, suturing, surgical malleting, or oscillation, which cause patient discomfort. The current study applied this technique with minor surgical modification of the atrophic alveolar ridge model on the assumption that tissue healing and the repair process in the atrophic ridge might elicit tissue responses to OTM different from those that occur in sound alveolar bone.

The purpose of the study was to evaluate the effect of flapless osteoperforation on the rate of OTM toward the atrophic alveolar ridge, also its effect on the morphological and biological responses of the atrophic alveolar bone ahead of moving teeth.

MATERIALS AND METHODS

Eight adult male beagles (mean weight, 11.2 kg) were housed following the guidelines of Kyung Hee University Medical Center-Institutional Animal Care and Use Committee. This research was approved by the Institutional Animal Ethical Committee (No.16-036). The beagle model with atrophic alveolar ridge was established in both mandibular quadrants 8 weeks after third premolar extraction. The socket was healed without pathologic inflammation under the control of oral hygiene, accompanied by ridge constriction both buccolingually and vertically, and confirmed by standard x-rays and clinical measurement (Figure 1). As a split-mouth design, both quadrants were randomly divided into two groups: group C (control), OTM only; group OP (osteoperforation), OTM with flapless osteoperforation.

Reciprocal traction of the second and fourth premolars, which were adjacent to the atrophic ridge, was performed for 10 weeks (Figure 1). Orthodontic brackets (Tomy Co, Tokyo, Japan) were bonded on the buccal surfaces of the two premolars and passive 0.019×0.025-inch sectional stainless steel wires (Tru-Chrome SS, RMO, Denver, CO) were inserted. Nickel-titanium closed-coil springs (light force; 3M Unitek, Monrovia, Calif) were activated between the long hooks on each pair of teeth, exerting a force of 100 g per tooth. The appliances and force levels were checked and adjusted every 2 weeks to maintain consistency.

Osteoperforation was performed immediately before initiating OTM in group OP by cortical punching, passing through the overlying mucosa on the atrophic ridge. Multiple punching was done at nine points on the buccal side using a pilot drill (Bio Materials Korea, Seoul, Korea) with a diameter of 1.2 mm: three points close to the second premolar root, three close to the fourth premolar root, and three in the middle of the edentulous ridge (Figure 1). The depth of punching was confined to less than 3 mm to minimally invade

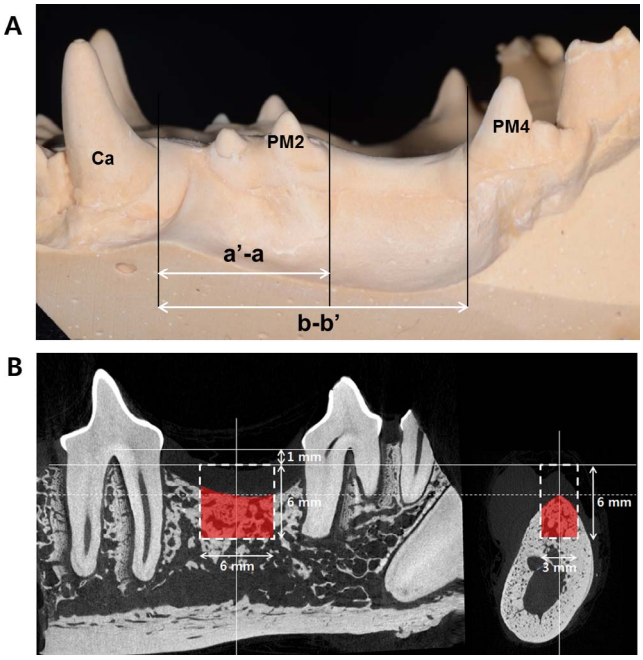

Figure 2. Methods of model measurement (A) and histomorphometric measurements on micro-CT images (B).

cancellous bone through the whole layer of cortical bone. For postoperative care, analgesics (Ketopro; Uni Biotech Co, Yesan, Korea) and antibiotics (gentamycin; Komipharm International Co, Shiheung, Korea) were administered intramuscularly bid for 3 days, and 0.12% chlorhexidine gluconate rinse (hexamedine solution; Bukwang Pharm Co, Seoul, Korea) was applied daily. All animals were euthanized by direct injection of 50 mL/kg Zoletil 50 (Virbac Lab, Carros, France) into the heart 10 weeks after OTM.

Amount of OTM was measured on precisely fabricated stone models taken every 2 weeks. The distances of second premolar movement (a′–a) and fourth premolar movement (b–b′) were measured separately and analyzed (Figure 2A): distance from distal cervix of canine to distal cervix of second premolar before movement (a) and at each observation time point (a′); distance from distal cervix of canine to mesial cervix of fourth premolar before movement (b) and at each observation time point (b′). All measurements were repeated twice by one investigator with an interval of 2 weeks, and the mean accumulated distance was compared between groups.

Tissue blocks including the atrophic ridge and the two moved teeth were harvested and immediately fixed by 10% formalin for 48 hours. Micro-CT images were taken using SkyScan 1173 (Bruker-microCT, Kontich, Belgium) with settings of 90 kVp source voltage, 88 mA of current, and 18.11μm of image pixel size. Color-mapped sectional images were obtained to indicate differential tissue density and calibrated by DataViewer (Bruker-microCT). Three-dimensional images were reconstructed using CTVox software (Bruker-microCT). To define a regional volume of interest (VOI), a cube of 6.0 × 6.0 × 3.0 mm was designated to confine the measuring area to the atrophic ridge, encompassing the central portion of the ridge between the two roots (Figure 2B). The upper reference of the cube constituted a parallel plane 1 mm below the plane connecting the cementoenamel junctions of the two teeth. Percentage bone volume (BV/cube %) was defined as the fraction of total bone volume within the designated VOI cube excluding the empty space. Within the total tissue volume, bone mineral density (BMD, g/cm^3), bone surface ratio (BS/BV, %), trabecular thickness (TbTh, mm), trabecular number (TbN, mm), and trabecular separation (TbSp, mm) were measured twice by one technician and automatically calculated into three-dimensional data sets as mean values (version 1.12.0.0, CT Analyzer; Bruker-microCT).

Tissue blocks from one beagle (n = 1/group) were prepared for total RNA extraction with the RNeasy mini kit (Qiagen, Valencia, Calif). RNA integrity was measured by using an Agilent 2100 Bioanalyzer (Agilent Technologies, Palo Alto, Calif), and a sample with an RNA integrity number (RIN) greater than or equal to 8 was considered to be of acceptable quality. Transcriptome sequencing was initiated by transforming mRNA in total RNA samples into a template library, followed by cluster generation using the components provided in the TruSeq Sample Preparation RNA Kit (Illumina, San Diego, Calif). Differentially expressed genes (DEGs) were defined as those with changes of at least twofold between a pair of samples, at a false discovery rate of 5%. Identified DEGs were clustered by the Mfuzz package in R using average normalized signal intensity values of individual genes as input values. The Kyoto Encyclopedia of Genes and Genomes (KEGG) database resource was used to find significant functional pathways and the contributing gene set. A filtered KEGG-enrichment heat map on the basis of KEGG pathway map IDs was extracted associated with DEGs between groups.

Statistical Analysis

Descriptive statistics were represented as means and standard deviations. Intraexaminer reliability was tested by intraclass correlation coefficient of 0.901 for the OTM distance and of 0.915 for the microstructural parameters between the measured sets. Based on the Kolmogorov-Smirnov normality test ($P < .05$), the Mann-Whitney *U* test was used to compare the rate of OTM and each microstructural parameter between

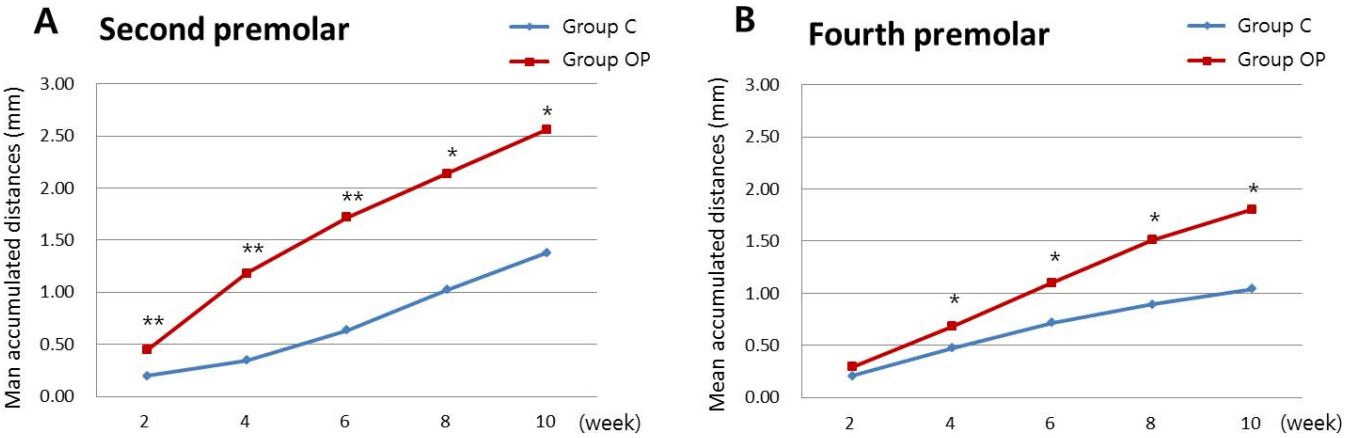

Figure 3. Graphs illustrating mean accumulated distance of the second premolar (A) and the fourth premolar (B). * $P < .5$; ** $P < .01$.

groups. Values of $P < .05$ were considered to indicate statistically significant differences.

RESULTS

Rate of OTM

The mean accumulated distances of the second and fourth premolars were significantly higher in group OP than in group C at all observation points (Figure 3). At 10 weeks post-movement, the mean distance of the second premolar in group OP (2.56 ± 0.94 mm) was 1.86 times that in group C (1.38 ± 0.06 mm), and the distance of the fourth premolar in group OP (1.81±0.43 mm) was 1.74 times that in group C (1.04 ± 0.52 mm).

Histomorphometric Findings

Micro-CT volume images exhibited no significant difference in atrophic ridge volume between groups (Figure 4A,D; Table 1). Half-volume sectional images (Figure 4B,E) represented no intergroup difference in vertical ridge level, but revealed a different trabecular pattern between groups, which could be confirmed by color-mapped longitudinal sections (Figure 4C,F). Group OP exhibited a high proportion of low density bone, marked by green and yellow colors on the ridge including the crestal bridge (Figure 4F). In contrast, group C showed a ridge crest composed of highly dense bone marked by the blue color (Figure 4C). Notably, bodily tooth movement occurred in group OP, identified by a parallel trace of newly formed bundle bone from the furcation to the apex on the tension side of moved roots (Figure 4F). Meanwhile, alveolar crest levels on the compression sides of moved teeth showed no remarkable differences between groups.

As a result of quantitative histomorphometric analysis, percentage bone volume and bone surface ratio exhibited no significant differences between groups (Table 1). However, group OP revealed lower bone mineral density ($P < .01$), higher trabecular number ($P < .05$), lower trabecular thickness ($P < .05$), and lower trabecular separation ($P < .05$) than did group C.

Gene Expression Profiling by RNA Sequencing Analysis

As a result of principal gene analysis, 10,113 gene transcripts with at least zero fragments per kilobase of exon per million fragments mapped (FPKMs) were excluded from 30,021 total extracted genes. High reproducibility between samples was indicated by a Pearson coefficient of 0.98 to see the degree of intersample similarity using $\log_2$ (FPKM+1) value. Out of the remaining 19,908 gene transcripts, 602 differentially expressed genes (DEGs) with statistical significance ($P < .05$) and fold changes ≥ 2 and ≤ -2 were finally sorted out (Figure 5A,B). Two hundred thirty genes were up-regulated and 372 were down-regulated in group OP compared with the control group (group C). A scatter plot revealed whole distribution of DEGs between groups (Figure 5C), and a volume plot identified specific genes with strong volume for high reliability in group OP vs group C (Figure 5D). In order of high volume of expressed genes in group OP, the five top-ranked genes were sorted out: ND4L, CTSK, ACP5 as up-regulated genes and APOD and CFD as down-regulated genes (Table 2). A filtered KEGG-enrichment analysis extracted the 20 top-ranked biological functional map IDs in group OP vs group C ($P < .001$): osteoclast differentiation, tumor necrosis factor (TNF) signaling pathway, AMP-activated protein kinase (AMPK) signaling pathway, Wnt signaling pathway, and extracellular matrix (ECM)-receptor interaction (Figure 6). In order of group OP/group C volume, the contributing gene set was sorted out in each pathway (Table 3).

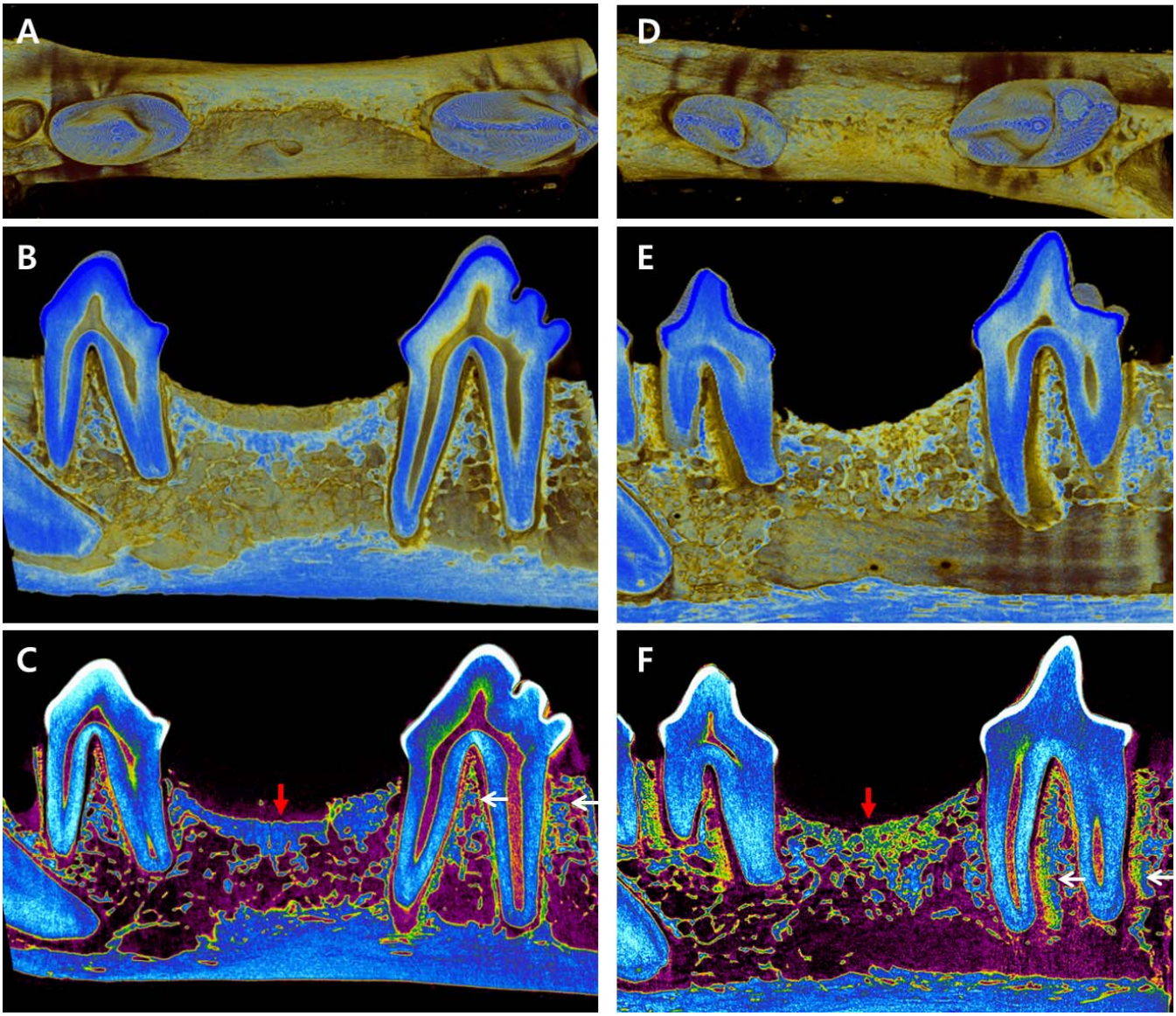

Figure 4. Micro-CT images of group C (A–C) and group OP (D–F). (A and D) occlusal view of volume images; (B and E) half-volume images showing trabecular pattern; (C and F) color-mapped sectional images indicating differential tissue density.

DISCUSSION

The present study elucidated that OTM could be facilitated by flapless osteoperforation through the atrophic alveolar ridge without dimensional improvement of the atrophic ridge. Previous research has attempted to establish clinically available evidence on minimally invasive surgical procedures, mostly in terms of accelerating tooth movement in sound periodontium.

Table 1. Intergroup Comparison of Six Microstructural Parameters Measured From a Designated Micro-CT Volume of Interest as a Result of Histomorphometric Analysis

Parameters	Abbreviation	Group C	Group OP	*P* Value
Bone volume fraction[a]	BV/cubic (%)	40.91 ± 2.53	42.77 ± 0.83	.292
Bone mineral density	BMD (g/cm^3)	0.77 ± 0.08	0.57 ± 0.02	.003**
Bone surface ratio	BS/BV (%)	5.16 ± 1.77	6.66 ± 1.41	.316
Trabecular thickness	TbTh (mm)	0.73 ± 0.08	0.43 ± 0.07	.010*
Trabecular number	TbN (mm^{-1})	0.62 ± 0.06	1.04 ± 0.13	.010*
Trabecular separation	TbSp (mm)	1.60 ± 0.11	1.28 ± 0.16	.048*

[a] Mean ± SD
Mann-Whitney *U* test. * $P < .5$; ** $P < .01$.

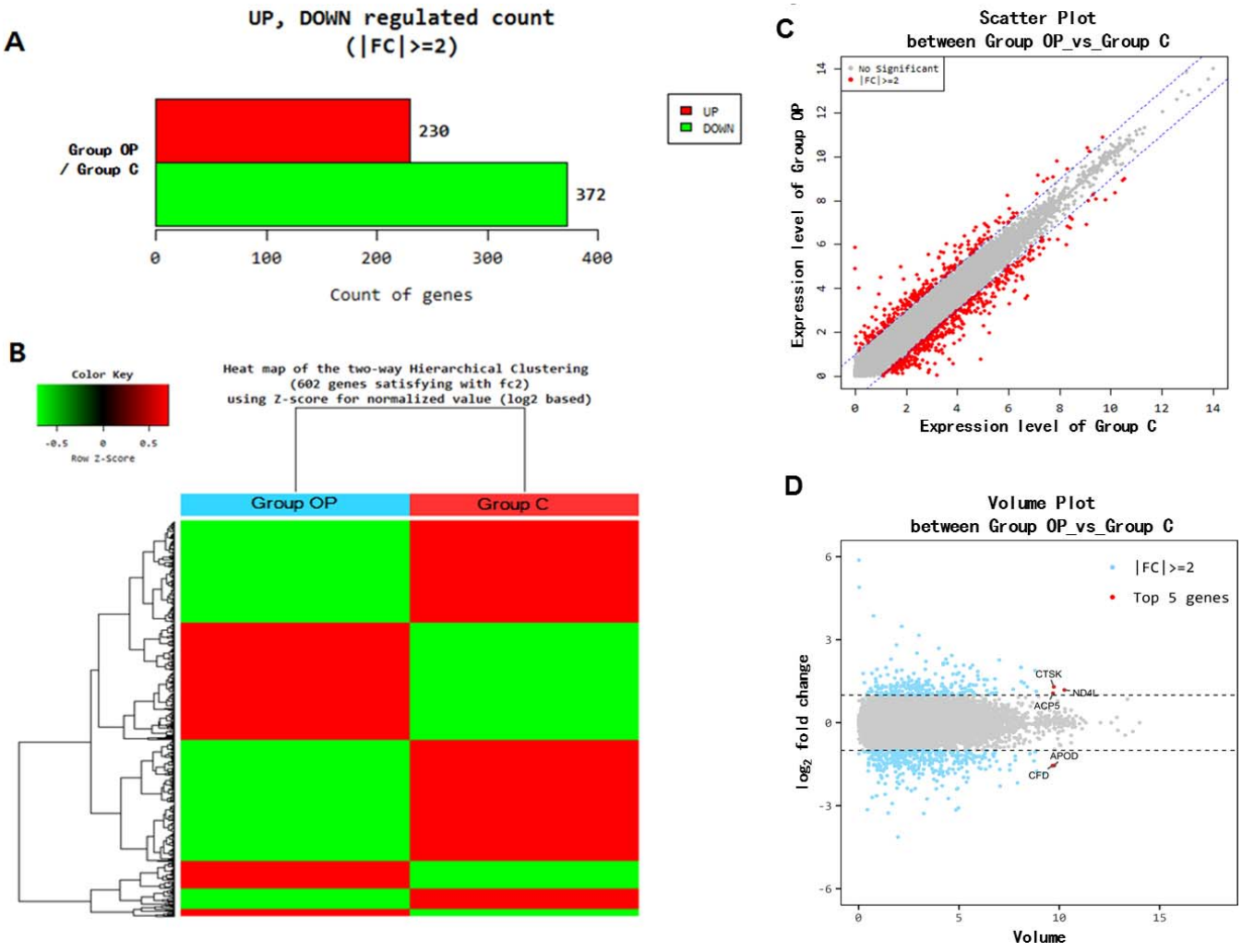

Figure 5. (A) Up- and down-regulated count of DEGs in group OP, with fold changes $\geq|2|$. (B) Hierarchical clustering heat map using Z-score for log_2-based normalized value. (C) Scatter plot of DEGs between groups. (D) Volume plot to identify specific genes with strong volume in group OP vs group C.

Teixeira et al.[11] suggested that OTM on day 28 after three micro-osteoperforations with flap surgery in rats was 2.13 times as fast as that of the control group. Baloul et al.[12] reported that OTM was 1.3 times as fast on day 42 after selective decortication with flap elevation in rats. Cho et al.[13] found that the amount of OTM increased to 4.41 times and 2.44 times in the maxilla and mandible, respectively, after applying 24 decortication dots with flap surgery in dogs. Tsai et al.[14] found that the rate of OTM was 1.54 and 1.49 times as fast in a corticision group and micro-osteoperforation group, respectively, than in the control, showing no difference between the two flapless procedures. In the current study, it was found that flapless osteoperforation facilitated OTM by 1.81 times even through the atrophic ridge in the beagle mandible over 10 weeks.

Table 2. Descriptions of the Five Top-Ranked Differentially Expressed Genes From Volume Plotting Between Groups ($P < .001$)

Gene Symbol	Description	Fold Change	Volume[a]
ND4L	NADH dehydrogenase subunit 4L	2.28	10.25
APOD	Apolipoprotein D	−2.91	9.74
CTSK	Cathepsin K	2.46	9.72
ACP5	Acid phosphatase 5, tartrate resistant (TRAP)	2.09	9.68
CFD	Complement factor D	−2.93	9.65

[a] Volume indicates square root (control normalized value×test normalized value).

In terms of morphological alterations of the atrophic ridge ahead of the surgically facilitated tooth movement, neither increment nor decrement of the ridge dimension was observed when flapless osteoperforation was performed, even without the flap reflection that might develop residual ridge resorption.[15] On the other hand, transient local osteoporotic change induced by

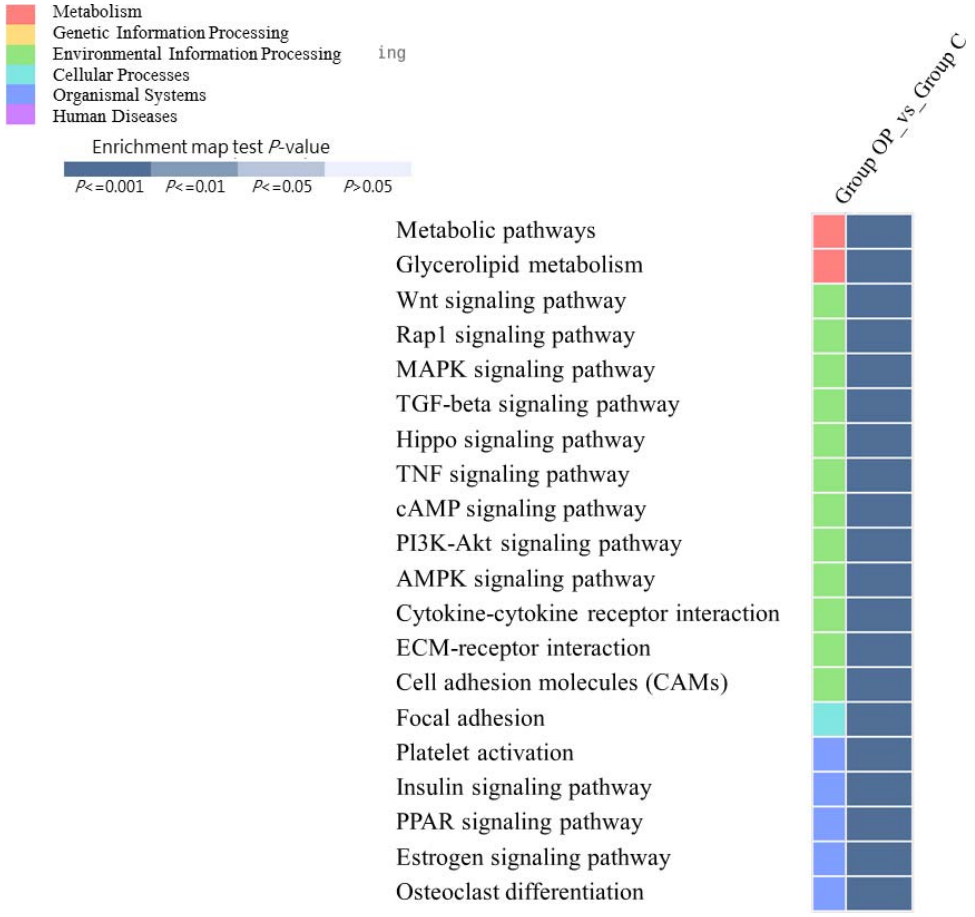

Figure 6. A filtered KEGG-enrichment heat map on the basis of KEGG pathway map IDs associated with DEGs between groups; 20 top-ranking map IDs were extracted ($P < .001$).

RAP with increased osteoclastic, osteoblastic, and fibroblastic activities was observed in the atrophic ridge model, as supported by histomorphometric and gene-enrichment analysis.

Few studies have demonstrated the underlying biological mechanisms of surgically assisted tooth movement, particularly at the gene level. Introducing RNA sequencing analysis, bone-related specific functional pathways, and the contributing genes induced by osteoperforation were elucidated. The final count of DEGs between groups was 3% of all the tested genes, with 38% of up-regulated and 62% of down-regulated genes in group OP. Among the five top-ranking genes with strong volume in group OP/group C combination, CTSK (cathepsin K) and ACP5 (acid phosphatase 5) genes are well-established biological markers reflecting osteoclast differentiation and activation. The protein encoded by CTSK is a lysosomal cysteine protease involved in bone remodeling and repair,[16] and ACP5 is associated with osteoclast migration, differentiation, activation, and proliferation.[17] Based on the filtered KEGG-enrichment maps, the TNF signaling pathway, participating in inflammatory bone resorption by stimulating ligand for receptor activator of NF-κB-induced osteoclastogenesis, was significantly up-regulated in group OP,[18] wherein matrix metalloproteinase 9 (MMP-9) and IL-6 genes were up-regulated (Table 3). MMP-9 degrades bone collagen in concert with MMP-1 and cysteine proteases,[19] and IL-6 acts on osteoclastogenesis and bone resorption.[20] With the activation of CTSK and ACP5 mentioned above, the up-regulated TNF signaling pathway might contribute to low bone density within the ridge at 10 weeks after OTM by osteoperforation. Accordingly, the AMPK signaling pathway, as a key sensing mechanism in regulating osteogenesis,[21] and the Wnt signaling pathway, which affects bone modeling and remodeling by stimulating osteogenesis,[22] were down-regulated in group OP, which might support the findings of less mature woven bone without appositional bone modeling on the atrophic ridge by osteoperforation. Additionally, the up-regulated ECM-receptor interaction in group OP included increased expression of the fibronectin (FN1), integrin alpha 2 (ITGA2), and integrin beta 3 (ITGB3)

Table 3. Five Top-Ranked Differentially Expressed Genes Associated With KEGG Pathway

KEGG Pathway	Gene Symbol	Description	Fold Change	Volume
Osteoclast differentiation	CTSK	Cathepsin K	2.46	9.7191
(map ID 04380)	ACP5	Acid phosphatase 5, tartrate resistant	2.09	9.6760
	FOSL2	FOS-like antigen 2	2.24	5.5032
	ITGB3	Integrin, beta 3 (antigen CD61)	2.61	4.6275
	TNFRSF11A	Tumor necrosis factor receptor superfamily member 11A	2.54	2.9885
TNF signaling pathway	MMP-9	Matrix metallopeptidase 9 (gelatinase B)	2.46	8.3908
(map ID 04668)	CCL5	CHEMOKINE (C-C MOTIF) LIGAND 5	2.66	2.9296
	CCL20	Chemokine (C-C motif) ligand 20	3.15	2.4774
	IL6	Interleukin 6 (interferon, beta 2)	11.17	2.1423
	MMP-3	Matrix metallopeptidase 3 (stromelysin 1)	−2.50	1.0399
AMPK signaling pathway	SCD	ACYL-COA DESATURASE	−4.51	7.9036
(map ID 04152)	ADIPOQ	Adiponectin, C1Q and collagen domain-containing	−3.22	7.0321
	LIPE	Hormone-sensitive lipase	−3.07	5.1321
	STRADB	STE20-related kinase adapter protein beta	2.37	3.7338
	IGF1	Insulin-like growth factor 1 (somatomedin C)	3.81	3.3111
Wnt signaling pathway	SOST	Sclerostin	2.04	6.5065
(map ID 04310)	SFRP1	Secreted frizzled-related protein 1	−3.17	4.0707
	SOX17	Trnscription factor SOX-17	−4.12	3.7474
	PLCB2	1-Phosphatidylinositol 4,5-bisphosphate phosphodiesterase b-2	2.05	3.4806
	CAMK2A	Calcium/calmodulin-dependent protein kinase II α	−2.19	1.6629
ECM-receptor interaction	FN1	Fibronectin	2.31	7.6960
(map ID 04512)	ITGB3	Integrin beta 3 (platelet glycoprotein IIIa)	2.61	4.6276
	THBS4	Thrombospondin 4	−4.85	4.1539
	COL27A1	Collagen alpha-1(XXVII) chain	2.05	3.6663
	ITGA2	Integrin alpha-2	4.91	1.5972

genes related to increased ECM formation and a kind of collagenase (COL27A1) gene to keep the tissue organization process in balance.

It should be noted that gene expression in beagles is not sufficiently informative because of interspecies or intraspecies genetic variations and lack of a well-established gene bank. Tissues for RNA extraction were harvested from one animal to compensate for interindividual genetic variation, since increasing sample size could cause interpretation errors from the mixed samples. Nonetheless, a large animal was required for the purpose of comparing tissue responses and dimensions as a preclinical study. With further study to verify the function of DEGs, specific biological modulators to control the rate of tooth movement with periodontal improvement could be elucidated.

CONCLUSIONS

- Flapless osteoperforation facilitated the rate of OTM toward the atrophic ridge, maintaining lowered bone density for 10 weeks.
- However, it did not increase the volume of the ridge. These observations were supported by RNA sequencing that sorted out top-ranking DEGs from up- and down-regulated biological pathways induced by osteoperforation.

ACKNOWLEDGMENT

This study was supported by a National Research Foundation (NRF) grant funded by the Korean government (2014R1A1A3052072).

REFERENCES

1. Araújo MG, Lindhe J. Dimensional ridge alterations following tooth extraction. An experimental study in the dog. *J Clin Periodontol*. 2005;32:212–218.
2. Nevins M, Camelo M, De Paoli S, Friedland B, Schenk RK, Parma-Benfenati S, et al. A study of the fate of the buccal wall of extraction sockets of teeth with prominent roots. *Int J Periodontics Restorative Dent*. 2006;26:19–29.
3. Araújo MG, Carmagnola D, Berglundh T, Thilander B, Lindhe J. Orthodontic movement in bone defects augmented with Bio-Oss: an experimental study in dogs. *J Clin Periodontol*. 2001;28:73–80.
4. Wilcko MT, Wilcko WM, Pulver JJ, Bissada NF, Bouquot JE. Accelerated osteogenic orthodontics technique: a 1-stage surgically facilitated rapid orthodontic technique with alveolar augmentation. *J Oral Maxillofac Surg*. 2009;67:2149–2159.
5. Zhang D, Chu F, Yang Y, Xia L, Zeng D, Uludağ H, et al. Orthodontic tooth movement in alveolar cleft repaired with a tissue engineering bone: an experimental study in dogs. *Tissue Eng*. Part A. 2011;17:1313–1325.
6. Kim SJ, Park YG, Kang SG. Effects of corticision on paradental remodeling in orthodontic tooth movement. *Angle Orthod*. 2009;79:284–291.
7. Dibart S, Sebaoun JD, Surmenian J. Piezocision: a minimally invasive, periodontally accelerated orthodontic

tooth movement procedure. *Compend Contin Educ Dent*. 2009;30:342–344, 346, 348–350.
8. Kim YS, Kim SJ, Yoon HJ, Lee PJ, Moon W, Park YG. Effect of piezopuncture on tooth movement and bone remodeling in dogs. *Am J Orthod Dentofacial Orthop*. 2013;144:23–31.
9. Alikhani M, Raptis M, Zoldan B, Sangsuwon C, Lee YB, Alyami B, et al. Effect of micro–osteoperforations on the rate of tooth movement. *Am J Orthod Dentofacial Orthop*. 2013;144:639–648.
10. Cheung T, Park JY, Lee D, Kim C, Olson J, Javadi S, et al. Ability of mini-implant-facilitated miro-osteoperforations to accelerate tooth movement in rats. A*m J Orthod Dentofacial Orthop*. 2016;150:958–967.
11. Teixeira CC, Khoo E, Tran J, Chartres I, Liu Y, Thant LM, et al. Cytokine expression and accelerated tooth movement. *J Dent Res*. 2010;89:1135–1141.
12. Baloul SS, Gerstenfeld LC, Morgan EF, Carvalho RS, Van Dyke TE, Kantarci A. Mechanism of action and morphologic changes in the alveolar bone in response to selective alveolar decortication–facilitated tooth movement. *Am J Orthod Dentofacial Orthop*. 2011;139:S83–S101.
13. Cho KW, Cho SW, Oh CO, Ryu YK, Ohshima H, Jung HS. The effect of cortical activation on orthodontic tooth movement. *Oral Dis*. 2007;13:314–319.
14. Tsai CY, Yang TK, Hsieh HY, Yang LY. Comparison of the effects of micro-osteoperforation and corticision on the rate of orthodontic tooth movement in rats. *Angle Orthod*. 2016;86:558–564.
15. Yaffe A, Fine N, Binderman I. Regional accelerated phenomenon in the mandible following mucoperiosteal flap surgery. *J Periodontol*. 1994;65:79–83.
16. Helali AM, Iti FM, Mohamed IN. Cathepsin K inhibitors: a novel target but promising approach in the treatment of osteoporosis. *Curr Drug Targets*. 2013;14:1591–1600.
17. Sheu TJ, Schwarz EM, Martinez DA, et al. A phage display technique identifies a novel regulator of cell differentiation. *J Biol Chem*. 2003;278:438–443.
18. Boyce BF, Xing L. Functions of RANKL/RANK/OPG in bone modeling and remodeling. *Arch Biochem Biophys*. 2008;473:139–146.
19. Okada Y, Naka K, Kawamura K, Matsumoto T, Nakanishi I, Fujimoto N, et al. Localization of matrix metalloproteinase 9 in osteoclasts: implications for bone resorption. *Lab Invest*. 1995;72:311–322.
20. Udagawa N, Takahashi N, Katagiri T, Tamura T, Wada S, Findlay DM, et al. Interleukin (IL)-6 induction of osteoclast differentiation depends on IL-6 receptors expressed on osteoblastic cells but not on osteoclast progenitors. *J Exp Med*. 1995;182:1461–1468.
21. Wang Y, Fan Q, Tang T. The regulatory role of AMPK signaling pathway in bone metabolism. *Chin J Osteoporos*. 2014;20:322–326
22. Wang Y, Li YP, Paulson C, et al. Wnt and the Wnt signaling pathway in bone development and disease. *Front Biosci*. 2014;19:379–407.